BLAST AND FRAGMENT CONTAINMENT CAPABILITY OF PORTABLE CHAMBERS

BATTELLE COLUMBUS LABORATORIES

PREPARED FOR

NAVAL EXPLOSIVE ORDNANCE DISPOSAL FACILITY

SEPTEMBER 1975

NAVEODFAC TECHNICAL REPORT TR-172

BLAST AND FRAGMENT CONTAINMENT CAPABILITY OF PORTABLE CHAMBERS

by

B.D.Trott,

J.E. Backofen, Jr.,

and

J.J. White, III

BATTELLE

Columbus Laboratories

505 King Avenue

Columbus, Ohio 43201

September 1975

FINAL REPORT

Prepared for

NAVAL EXPLOSIVE ORDNANCE DISPOSAL FACILITY

Indian Head, Maryland 20640

Released by
LIONEL A. DICKINSON
Technical Director

Under Authority of
J.R. HECK, CDR, USN
Commanding Officer

SECURITY CLASSIFICATION OF THIS PAGE (When Data Entered)

REPORT DOCUMENTATION PAGE

READ INSTRUCTIONS BEFORE COMPLETING FORM

1. REPORT NUMBER: TR 172	2. GOVT ACCESSION NO.
3. RECIPIENT'S CATALOG NUMBER	
4. TITLE (and Subtitle): BLAST AND FRAGMENT CONTAINMENT CAPABILITY OF PORTABLE CHAMBERS	5. TYPE OF REPORT & PERIOD COVERED: Final Report Feb. 7, 1974 — Sept. 8, 1975
	6. PERFORMING ORG. REPORT NUMBER
7. AUTHOR(s): B. Dale Trott, Joseph E. Backofen, Jr. and John J. White, III	8. CONTRACT OR GRANT NUMBER(s): Contract No. N00174-74-C-0219
9. PERFORMING ORGANIZATION NAME AND ADDRESS: Battelle Columbus Laboratories 505 King Avenue Columbus, Ohio 43201	10. PROGRAM ELEMENT, PROJECT, TASK AREA & WORK UNIT NUMBERS: Program Element 62734N Project 8F-34-373
11. CONTROLLING OFFICE NAME AND ADDRESS: Naval Explosive Ordnance Disposal Facility Indian Head, Maryland 20640	12. REPORT DATE: September 1975
	13. NUMBER OF PAGES: 57
14. MONITORING AGENCY NAME & ADDRESS(if different from Controlling Office)	15. SECURITY CLASS. (of this report): Unclassified
	15a. DECLASSIFICATION/DOWNGRADING SCHEDULE

16. DISTRIBUTION STATEMENT (of this Report)

Approved for public release; distribution unlimited.

17. DISTRIBUTION STATEMENT (of the abstract entered in Block 20, if different from Report)

18. SUPPLEMENTARY NOTES

19. KEY WORDS (Continue on reverse side if necessary and identify by block number)

Explosion Containment Vessels
Blast Containment Vessels
Explosive Ordnance Disposal
Fragment Restraint Systems

20. ABSTRACT (Continue on reverse side if necessary and identify by block number)

It was found that a 2-inch annulus of sand surrounding a C-4-filled, 2-inch-diameter pipe was sufficient to prevent the formation of fragment craters on the inside of a blast/fragment containment chamber. This fragment restraint system was demonstrated in a series of explosive tests in a 2-foot-diameter, 0.5-inch-wall, spherical blast containment chamber designed and fabricated for this investigation. It was also found that bare cylindrical charge shapes lead to greater local strains in a spherical vessel in the plane normal to the charge axis than equal weight spherical charges, while the metal- and sand-encased charges produced even greater plastic deformation of the containment vessel. The complete results of the fragment restraint studies, and a series of 10 explosive containment experimental shots are given. An analytical

(Continued)

DD FORM 1 JAN 73 1473 EDITION OF 1 NOV 65 IS OBSOLETE S/N 0102-014-6601

UNCLASSIFIED

SECURITY CLASSIFICATION OF THIS PAGE (When Data Entered)

model for the elastic-plastic deformation of the chamber showed good agreement with that observed for the bare spherical charges fired in the chamber.

PREFACE

Mr. Lennard Wolfson of the Naval Explosive Ordnance Disposal Facility served as Technical Monitor on this program. The many helpful discussions with him and his contribution of several good ideas to this program are gratefully acknowledged. Several persons on the Battelle staff also contributed to the success of this program. Worthy of mention are Joe H. Brown for managerial support, A. S. Chace for technical assistance, H. W. Mishler for establishment and supervision of the welding procedures used in the fabrication of the containment chamber, W. H. Stefanov, and others of the welding laboratory for conduct of the welding, J. W. Neutzling, H. C. Burchfield and others of the machine shop for fabrication and fit-up of the vessel parts, W. Scola, S. C. Green and J. L. White for assistance in the conduct of the explosive experiments, and E. C. Nowell for the principal typing work.

TABLE OF CONTENTS

TABLE OF CONTENTS
(Continued)

LIST OF TABLES

LIST OF FIGURES

TABLE OF CONTENTS
(Continued)

LIST OF FIGURES

THE BLAST AND FRAGMENT CONTAINMENT CAPABILITY OF PORTABLE CHAMBERS

by

B. D. Trott, J. E. Backofen, Jr., and J. J. White, III

INTRODUCTION AND SUMMARY

The objectives of this program were

- Development of a lightweight, expendable fragment restraint system to prevent localized damage to the interior of an explosion containment chamber from the explosion of explosive-filled, capped pipe sections ("pipe bombs").
- Development of blast response data for a small portable explosion containment chamber to include the effects of charge weight and charge shape in the form of cylinders from compact to long (length/diameter ratios from ~ 1 to ~ 8).
- Development of combined blast and fragment response data on the portable chamber from pipe bombs with the fragment restraint system in use.

All of the above objectives of this program were fulfilled.

An effective lightweight system capable of preventing the production of fragment craters from pipe bombs on the interior of containment chambers was found. It consisted of an annulus of common sand ~ 2-2.5 in. in thickness surrounding the pipe bomb, and in contact with it, or with an air gap up to 1-1/4 in. for 2 in. diameter Schedule 40 pipe. This system was not optimized during this program and further studies are in progress to determine the minimum sand layer requirements for various size pipe bombs.

A 2-ft diameter spherical steel explosion containment chamber was designed, and three such chambers were fabricated for this program. One was extensively tested and two were delivered as prototypes. The chambers are caster-wheel-mounted, have ~ 0.5 in. wall thickness and weigh ~ 400 lbs.

For spherical charges, good agreement with computer program predictions of residual plastic strain was obtained for 1.5 and 2.5 lb charges. The predictions in agreement with experiment used an 80,000 psi yield strength model for the vessel material.

For long bare cylindrical charges, strong anisotropic effects were observed. The containment chamber strain opposite the sides of the charges was much larger than that opposite the charge ends.

For pipe bombs with the fragment restraint system the anisotropic strain effects on the chamber were also large. In addition, it was found that 1.5 lb explosive charges in pipe bombs with a sand restraint system for the fragments produced significantly greater plastic strains than equivalent bare charges. Nevertheless the portable chamber demonstrated a significant containment capability for several repeated charges of this weight with no interior surface disturbances from fragment impact with the new fragment restraint system.

This report is divided into sections describing the design of the containment chamber, development of the fragment restraint system, and the explosive containment experiments with the results of testing.

CHAMBER DESIGN AND FABRICATION

Containment Chambers

Three portable blast containment vessels were fabricated for this program. They were spherical vessels with a single pin supported closure port. This design was based on an earlier Battelle design fabricated in a larger size vessel for Picatinny Arsenal.[1]* The chosen diameter and wall thickness were based on the considerations that the vessels should be sufficiently portable to allow them to be moved through standard 30-inch wide office doorways, transported on passenger elevators, and that they be capable of containing the blast and fragments from a 2-in.-diameter by 12-in.-long composition C-4 filled pipe bomb. The diameter selection of 2 feet was dictated by passage through the doorway and the size of commercially available hemispherical shells. The wall thickness selection was based on the fabrication of the maximum strength chamber commensurate with the requirements for portability

Figure 1 shows the schematic side view of the vessels, drawn to scale. The idea for the single-pin door support used in this design originated with Mr. Jon Petty of Picatinny Arsenal and was developed to its present form by the first two authors of this report. The operation of the single-pin door mechanism is given in the following paragraphs.

The adjusting bolts shown in Figure 1 are initially adjusted, together with the operating nut on the main pin, to provide a good fit of the door against the inside of the reinforcing ring. Free play built into the cross-pin allows the two adjusting bolts to bring both sides of the door into contact with the reinforcing ring. The block attached to the bottom of the support pin and the built-up box which surrounds the block and is welded to the door are designed to hold the door at only a slightly smaller angle to the main pin than the fully seated position. The adjusting bolts only provide for the final seating of the door against the ring by rotation of the door on the cross pin.

---

* References are listed at the end of this report.

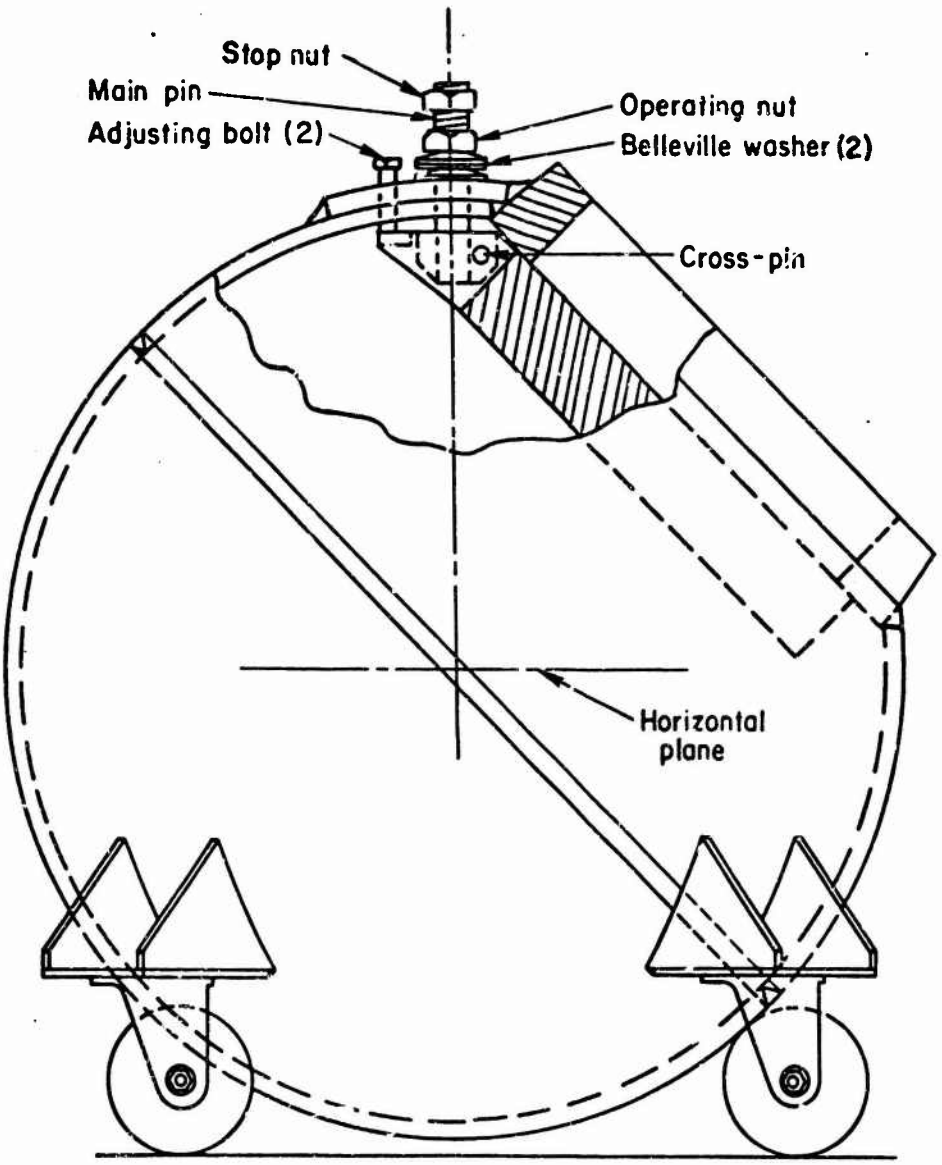

FIGURE 1. SCHEMATIC SIDE VIEW OF SPHERICAL CONTAINMENT VESSEL WITH SINGLE-PIN DOOR SUPPORT MECHANISM

The stop nut is also initially adjusted to allow the door to rotate around the inside of the vessel with small clearance when the operating nut is backed off against it. The stop nut is then locked in place on the main pin with Loctite.

With these initial adjustments made, and the door closed, as shown in Figure 1, the door is opened simply by rotation of the operating nut. The door is lowered for clear rotation initially, then further rotation of the operating nut, now against the stop nut, forces rotation of the main support pin and door through ~90 deg to the open position.

To close the door, the operating nut is merely rotated in the opposite direction. The door is rotated to its closed position by the initial rotation of the operating nut because of the jamming action of the stop nut and operating nut together. When the door rotates to its proper position to close completely, it contacts a door stop attached to the reinforcing ring. Continued rotation of the operating nut frees it from the stop nut and raises the door to the fully closed position. As the door rises, the adjusting bolts are again contacted and bring the door to an accurate seat angle against the ring.

As shots were fired in the vessel, it was only necessary to readjust the adjusting bolts to reestablish a good seating of the door against the reinforcing ring to compensate for the change in vessel shape due to the expected plastic stretching of the vessel. In the vessel evaluated during this program this door mechanism continued to operate satisfactorily after the last shot of the series was fired. At this point the vessel had suffered local strains in excess of 10 percent and an average plastic strain of just over 4 percent.

Material Selection

Steel was selected as the vessel material on the basis of cost, strength, fabricability, and availability. The selection of a specific grade of steel for the primary vessel was based on five considerations: (1) a high level of toughness, as measured by the Charpy notch-bar impact test, at low ambient temperature, (2) weldability, (3) cost, (4) availability,

and (5) the fact that steels with good impact properties at low temperatures must be good-quality steels. This provides additional assurance that deformation of the steels will not be adversely affected by unacceptable defects or improper processing.

The first choice steel grade selected is designated as ASTM A-537-72A, Class 1, or as ASME boiler steel SA-537A. This is a high-quality carbon steel with a nominal composition of 0.15 to 0.2 percent carbon, 1.2 percent manganese, 0.2 percent silicon, less than 0.02 percent sulfur, and less than 0.01 percent phosphorus. This steel, as specified by the American Society for Testing Materials (ASTM) or the American Society for Mechanical Engineers (ASME) boiler code, will have a minimum yield strength of 50,000 psi and elongation in 8 in. of 18 percent. In addition, this steel will have a guaranteed minimum Charpy notched-bar impact strength value of 12-ft-lb at a temperature of -75 F, a temperature far below expected ambient temperatures. Nominal values for impact strength at -75 F are about 30 ft-lb, and at -50 F about 55 ft-lb. This is a steel characterized by high levels of toughness even in the normalized heat-treatment condition (Class 1) that was specified for the vessel. This type of heat treatment was specified because it only requires heating to the specified temperature for the correct length of time and air cooling as compared with the more complicated heat treatments involving heating, quenching, and tempering, which can yield higher levels of impact strength.

The materials for these vessels were selected on the basis of availability within the guidelines above. During the time of ordering these vessels (1974) steel availability was less than normal, and the best alternate material available for the hemispheres was a steel designated as ASTM A-516 grade 70. This material is quite similar to A-537 but a lower yield strength is allowable, and low-temperature toughness is not normally guaranteed. However, the supplier of the hot-pressed hemispheres, Lukens Steel Co., did provide additional low-temperature Charpy impact property guarantees on the lot of A-516 Grade 70 material used for these vessels. The rings and doors for these vessels were fabricated from a section of 5-in.-thick plate of A-537-72B, Class 2 material. This was the only material available in the required sizes which fit the mechanical property requirements. This material is identical to A-537-72A, Class 1, except that it is supplied in the quenched

and tempered condition and is somewhat stronger than the normalized material.

Vessel Wall Thickness

Figure 2 shows results of an ultrasonic wall thickness survey conducted on vessel number 1. Assuming circular symmetry of each hemisphere, the weighted average thickness of this vessel was calculated to be 0.514 in. It will be noted that the minimum vessel thickness occurs not at the pole opposite the port but in a small circle surrounding the pole.

Table 1 gives measured wall thicknesses of Vessels 2 and 3. The four measurements at each location identified were taken at equally spaced locations around the periphery of the vessels before welding. No ultrasonic thickness surveys were made on these vessels.

Fabrication and Welding

The vessels were procured as hot-pressed hemispheres with the edges cut back and machined as a weld preparation so that when two hemispheres were welded together they would form the best possible sphere.

The initial step in fabrication was the machining of the hole for the port from one hemisphere, and cutting the doubler plate from the removed spherical piece. The reinforcing ring and doubler plate were then welded on to the hemisphere in the Battelle-Columbus Welding Development Laboratory. After this operation, the holes were drilled and tapped as necessary for the support pin and adjusting bolt. The door and door support parts were then assembled into the hemisphere-ring assembly and welded in place to assure proper alignment of all parts. Finally the main girth weld was completed in the Welding Development Laboratory.

The same welding procedure was used in making the welds between ring and vessel and the main girth weld. This procedure, No. P-75-A is included as Appendix B.

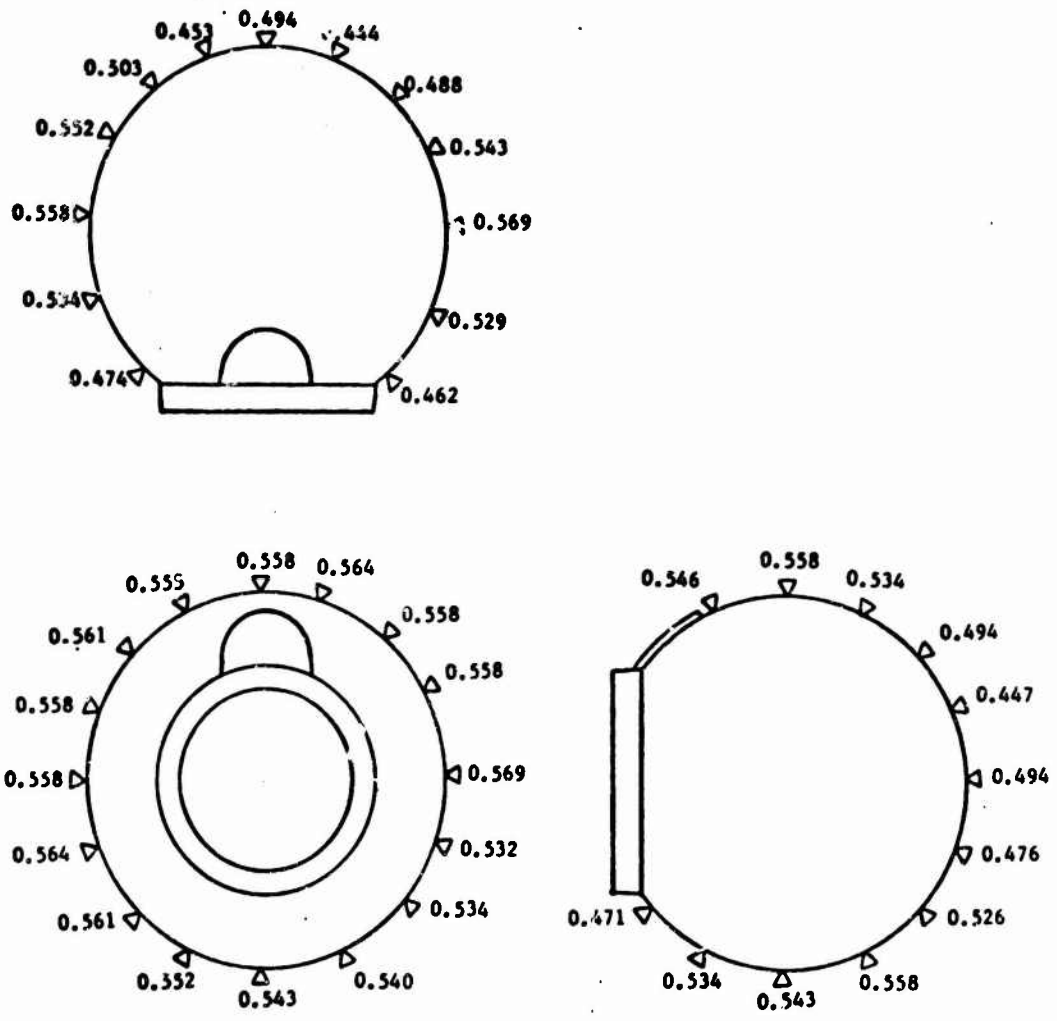

FIGURE 2. ULTRASONIC THICKNESS MEASUREMENTS
(All measurements are in inches)

TABLE 1. MEASUREMENTS OF WALL THICKNESSES OF VESSELS 2 AND 3
(All measurements are in inches)

Vessel No.	Lower Hemisphere, Adjacent to Weld	Upper Hemisphere	
		Adjacent to Weld	Adjacent to Port
2	0.534	0.540	0.463
	0.548	0.540	0.476
	0.543	0.530	0.468
	0.530	0.528	0.467
3	0.547	0.535	0.465
	0.554	0.536	0.464
	0.543	0.525	0.465
	0.530	0.533	0.456

A preheat temperature of at least 250 F was used prior to any welding. The steps following preheat were as follows:

- The ports to be welded were tacked in place using E-8016-C3 covered electrode.
- The root pass was deposited from the vessel inside surface using the shielded-metal-arc process and E-8016-C3 covered electrode.
- The root bead was ground out to sound metal from the outside.
- The ground surface of the root pass was dye-penetrant-inspected to insure removal of any lack of fusion in the base of the root pass. Areas showing any indication of lack of fusion were reground and rechecked until sound metal was ensured.
- The second weld pass was deposited from the outside by shielded metal arc using the same electrode material.
- The joint was completed using Hobart FabCO 81 cored wire electrode in a semi-automatic gas metal-arc welding process.
- The face of each pass was cleaned by power wire brushing to remove slag between welding passes.
- The completed joint was radiographically inspected according to Section VIII, Pressure Vessel Division 1 of the ASME Boiler and Pressure Vessel Code, 1974.

On the girth weld, the vessels were mounted on a rotating fixture after tacking to allow all welds to be deposited in the flat position.

Vessel Component Part Design

Ring and Door Design

The design criteria for the reinforcing ring and door have been given in detail in a previous report.[1] For this work the ring design was based on a vessel wall thickness of 0.550 inches, slightly over what the vessel average wall thickness measured when the hemispheres were delivered.

Following the steps in the design as given in reference 1, the radial overlap of the door and ring was chosen at 0.625 in. so that the bearing stress between the ring and the door would remain below 50 ksi for an apparent 100 ksi stress level in the vessel wall. The bearing surface was later reduced to a ring of 0.5 inch width during the design iteration of the reinforcing ring geometry, thus raising the bearing stress level to 54 ksi for an apparent 100 ksi stress level in the vessel wall.

The vessel door thickness t_d was found from the following formula from reference 1.

$$t_d = \left[\frac{3}{4} (3 + \nu) \, a_o^2 / \left(a_s / t_s - \frac{1}{2} \left(\frac{3 + \nu}{1 - \nu} \right) \right) \right]^{1/2}$$

where ν = Poisson's ratio = 0.27

a_s = the radius to the median surface of the vessel wall

t_s = the thickness of the vessel wall

a_o = location of the bearing stress load line from the door to the ring.

The thickness of the door was found to be 2.234 inches based upon an a_o of 6.3 in. This value was rounded up to a nominal 2.25 in. thickness.

The first approximation of the ring cross sectional area was 4.04 square inches. However, the thick ring formula of reference 1 was immediately used to size the ring between a thickness of 1.50 and 1.75 inches. The cross section of the ring and the load line geometry between the sphere, door, and ring was then iterated on an engineering layout to arrive at the final design and shop drawings.

Single-Vertical-Pin Door Mechanism Design

The main pin was initially sized to support the off axis weight of an 80 lb door subjected to a ten times gravity acceleration. The 1.0 in. diameter pin was chosen as it kept the maximum combined tensile stress below 30 ksi. The pin was more than sufficient to hold the door in place statically against the ring.

An allowable bearing stress of 20 ksi was chosen for surfaces of the main pin and its close-running-fit support hole. The bearing load P was given by the following formula:

$$P = k\, n\, W \Big/ \left[\left(t_s + t_d \right) - \left(2\, t/2 \right) \right] ,$$

where W = weight of the door

n = loading factor (10)

k = eccentricity of center of mass of the door from the center of the pin

t_s = thickness of the vessel wall

t_d = thickness of the doubler

t = thickness of the bearing surface

The formula for the bearing load was substituted into the following formula for the bearing stress σ_b to yield a quadratic expression that was solved to the required bearing surface thickness. Thus,

$$\sigma_b = P/td ,$$

where d = diameter of the pin.

When a single doubler made from the cutout of the hemisphere was used, the substitution of the values yielded a bearing thickness of 0.26 in.

A standard hex nut was chosen as having a sufficient pitch to provide easy opening and closing characteristics to the vessel, as well as having more than sufficient strength. The belleville washers were chosen to provide more than 1000 lb at 25 percent deflection and provide more than 0.025 in. residual deflection. Although one washer would be sufficient two were used to be conservative and flat hardened steel washers were placed

between them and the nut so that the door mechanism would still support the door even if one of the belleville washers popped over during the dynamic cycle of the vessel.

The cross pin was designed to transfer a 2800 lb load from the door to the main pin without the pin bending or the bearing surfaces of the pin yielding. The bending stress was calculated to be under 41 ksi and the maximum bearing stress under 15 ksi.

The remaining hardware was chosen conservatively based upon prior experience with the larger Picatinny vessel of similar design.

Location of Casters on the Vessel

Since the vessel was to be portable and roll freely into and out of elevators and doorways, large casters were welded to it so that a sufficient (2 in.) clearance would allow passage over small debris. It was then assumed that the vessel would be encountering door sills and the resulting action of the vessel was approximated by taking the kinetic energy of its prior horizontal motion and converting it to potential energy caused by the raising of the vessel center of mass as the vessel continued to move. In order for the forward motion of the vessel to stop when its centroid reached its maximum height, the vessel must be pushed no faster than 1.5 mph when the door is facing forward and 2.3 mph when the door is facing aft.

FRAGMENT RESTRAINT SYSTEM

In the search for a means to prevent the creation of internal craters on the containment vessel wall from fragment-producing metal-cased explosive charges, the idea of a system consisting of an additive mass surrounding the charge which would sufficiently slow the fragments without itself producing fragments was suggested by the program technical monitor, Mr. Lennard Wolfson of the Naval Explosive Ordnance Disposal Facility. This idea was selected for a preliminary investigation in this program.

A series of experiments to investigate the fragment attenuation capabilities of both water and ordinary sand were conducted to determine the thicknesses required to prevent the generation of craters inside the planned 2-ft-diameter vessel from the detonation of a 2-inch diameter pipe bomb filled with C-4. When favorable results were obtained from shots where the restraint medium was in contact with the bomb, the series was expanded to investigate the effect of an air gap adjacent to the pipe bomb in order to add design flexibility in the application of this concept. For this series, the water restraint medium was dropped from further study as it appeared to offer no advantages over the use of sand. Furthermore, a water restraint system including an air gap adjacent to the pipe bomb would be difficult to employ in the 2-ft diameter vessel.

The fragment restraint experiments were conducted in arenas comprised of a 2-3 foot section of large diameter pipe, lined with 1-ft-square witness plates. The pipe bombs utilized were C-4 filled 6-inch lengths of 2-in. schedule 40 pipe with a single end cap. In the first six experiments the open end of the bomb was left exposed. The surprisingly good results achieved prompted further investigation with the non-capped end of the pipe bomb restrained to eliminate the possibility that the detonation product gases were escaping from the unconfined end of the pipe bomb rather than pushing the pipe fragments to their full velocity.

Table 2 shows the first series of experiments with one end of the pipe bomb exposed and the results obtained, while Table 3 shows the second series of experiments which were identical except for covering the

Table 2. Summary of First Series of Mass Addition Fragment Restraint Experiments

Experiment Number	Restraint Mechanism: Material	In Contact or Air Gap, Inch	Thickness, Inch	Air Gap To Witness Plate, Inch	Results on Witness Plates
1	None	N/A	N/A	13.3	Peforated Radial Witness Plates & Split Arena Open
				9.0	~ 7/16" Craters in Witness Plate
2	Sand	In Contact	3.8 Radial	13.0	No Marks
			4.0 End Cap	9.0	No Marks
3	Water	In Contact	3.8 Radial	13.0	No Marks
			4.0 End Cap	9.0	No Marks
4	Sand	In Contact	2.3 Radial	14.5	Aluminum Stuck to Radial Witness Plates
			2.5 End Cap	9.0	No Marks
5	Sand	In Contact	1.8 Radial	15.0	No Marks
			2.0 End Cap	9.0	Small Indentations
6	Sand	0.37 Radial	2.5 Radial	14.0	No Marks
		0.50 End Cap	2.5 End Cap	9.0	No Marks

Table 3. Summary of Second Series of Mass Addition Fragment Restraint Experiments

Experiment Number	Material	Restraint Mechanism: In Contact or Air Gap, Inch	Material Thickness, Inch	Air Gap To Witness Plate, Inch	Results on Witness Plates
7	Sand	0.75 Radial	2.5	13.5	No Marks
		0.75 End Cap	2.5	9.0	No Marks
8	Sand	1.00 Radial	2.5	13.3	A Few Slight Dents
		1.00 End Cap	2.5	9.0	No Marks
9	Sand	1.25 Radial	2.5	13.0	No Marks
		1.25 End Cap	2.5	9.0	No Marks
10	Sand	1.25 Radial	2.0	13.5	No Marks
		1.25 End Cap	2.5	9.0	No Marks
11	Sand	0.37 Radial	2.0	9.0	No Marks
		0.13 End Cap	2.0	3.8	No Marks from Fragments but Bulge in (2) 0.25-Inch Witness Plates that were Suspended 0.275-inch above Floor

open end of the pipe with 0.020-in. aluminum sheet and 3 in. of sand.

Figure 3 shows the terminal effects of the radial fragments from experiment number 1. The bare pipe bomb was exploded in a round pipe arena with initially flat sections of 1/4 and 3/8-in. thick radial witness plates supported from it. A 3/4-in. witness plate backed up by several inches of steel was placed opposite the end cap. The fragments riddled the radial witness plates and produced stress concentrations great enough that the 29-in.-diameter, 3/8-in. thick arena split wide open, in a single axial crack to form a large "C" shape. The fragments from the end cap produced craters averaging about 7/16-in. in depth.

Figure 4 shows the 36-in.-diameter, 1/2-in. thick arena as it was set up for experiment number 2. This same set up geometry was also used for the subsequent tests listed in Tables 2 and 3. The restraining media was supported in a thin (0.020") aluminum cylinder. To support the water in experiment 3 a thin plastic liner was added to the aluminum cylinder.

Figure 5a shows the after experiment results of experiment 2. The witness plates consisted of single 3/8-in. thick mild steel or three layers of 1/8-in. thick mild steel. The plates were deformed to the curvature of the arena by the shot and covered with a very fine powder. No marks and/or indentations were observed on the witness plates.

Figure 5b shows the appearance of the witness plates from experiment 3 for comparison with the appearance of the witness plates shown in Figure 3.

The results of the second series of experiments demonstrate the validity of the use of sand as a fragment restraint system. This system was selected for use in the experiments conducted in the portable containment vessel described in the next section.

In summary the results found in these experiments are somewhat surprising in that velocities of up to 2500 ft/sec are predicted for the sand and fragments (experiment 5) using the Gurney cylindrical relationship. However, no fragment impressions were generated in the witness plates. A further research program is underway to determine the fragment crater reducing mechanism in more detail.

FIGURE 3. THREE 1/4-INCH WITNESS PLATES FROM EXPERIMENT NUMBER 1. THE WITNESS PLATES WERE APPROXIMATELY ONE FOOT SQUARE.

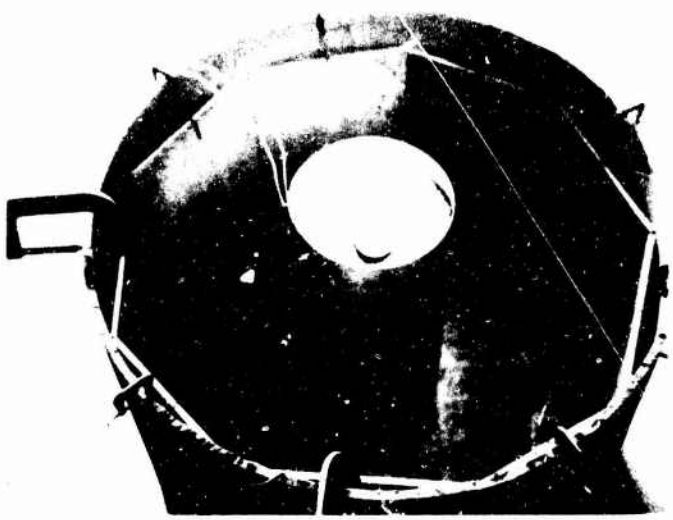

FIGURE 4. FRAGMENTATION ARENA FOR THE SAND MASS ADDITION FRAGMENT RESTRAINT EXPERIMENTS, EXPERIMENT NUMBER 2.

a. Witness Plates in Fragmentation Arena After Experiment Number 2

b. Appearance of Witness Plates from Experiment Number 3

FIGURE 5. APPEARANCE OF WATER-PROTECTED WITNESS PLATES.

EXPLOSIVE CONTAINMENT EXPERIMENTS

A series of 10 explosive containment experiments were conducted in one of the portable vessels. This section describes the diagnostics used to obtain data on the vessel performance, the shots fired in the chamber and the results obtained.

Instrumentation and Diagnostics

Two means were employed to follow the performance of the vessel. A series of 6 strain gages were installed on the vessel surface to follow both dynamic and static strains. To follow the plastic strains of the vessel a network of fiducial marks were placed on the vessel surface.

Figure 6 shows the location and orientation of the strain gages installed on the vessel. The rationale for their locations was as follows. Gage No. 1, was located near the ring to monitor a possible dynamic strain concentration in this location. Gage Nos. 2 and 3 were located near the weld and at the pole to monitor strains in these locations. Gage No. 4 was located on the ring to monitor ring hoop strains. Gage Nos. 5 and 6 were located intermediate between other gages. The gage numbering system follows that employed for gages installed at similar locations on previous blast containment work. The gages were Micro-Measurements' Type EA-06-250AE-350. Their installation using Baldwin-Lima-Hamilton EPY-500 epoxy cement followed the procedure given in reference 1.

They were monitored dynamically using a full bridge configuration completed with precision 350-ohm resistors and trimmed with a resistor decade box shunting one of the bridge completion legs. Each bridge was powered by 12 VDC from an automotive type wet cell battery. The bridge outputs were recorded directly on Tektronix Type 502A oscilloscopes. Strain calibration of the output was accomplished using the direct-shunt technique.[1]

The static strain on the gages was also monitored using a Vishay Instrument Model SB-1 Switch and Balance Unit and Budd Model P-350 Strain Indicator.

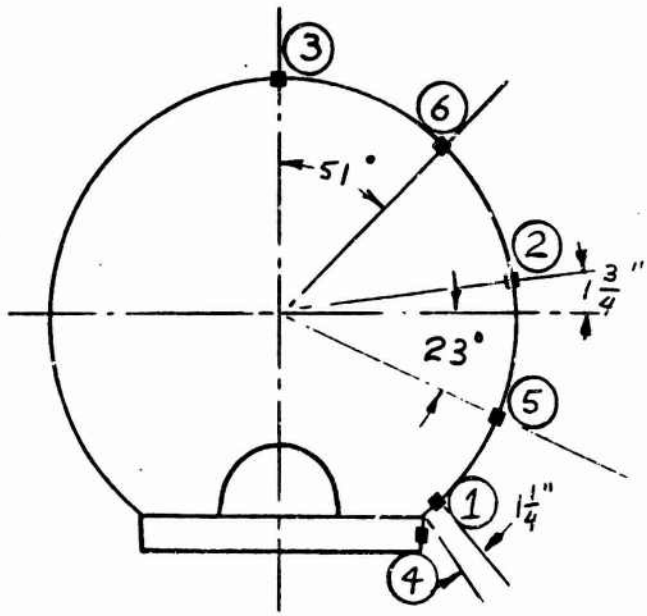

FIGURE 6. STRAIN GAGE LOCATIONS. THE MEASURING DIRECTION OF ALL GAGES EXCEPT #4 LIES IN THE PLANE OF THE FIGURE. GAGE #4 IS ARRANGED TO MEASURE THE HOOP STRAIN ON THE PORT REINFORCING RING.

Figure 7 shows the locations on the vessel surface of a series of fiducial marks. The marks consisted of prick-punch marks in the locations shown. The distance between marks on the vessel surface were measured before, between, and after all shots using a large dial-gage caliper equipped with sharp points to fit in the prick punch marks. Thus these measurements were actually of chord distances between marks rather than measurements along the vessel surface. The reproducibility of these measurements was generally ±0.005 in. or better. The marks on the surface of the reinforcing ring were sharply scribed lines. The distances between them were measured with the aid of an especially constructed steel scale with graduations to 0.01 inch. This scale was read with the aid of a hand-held lens providing measurements reproducible to at least ±0.005 inch.

Experimental Firings

Table 4 shows the series of ten test shots fired in the vessel. This test series included experiments designed to make a preliminary investigation of the following variables on the response of a completely closed containment chamber:

- effect of charge weight
- effect of steel wool as an energy absorber
- effect of a sand layer surrounding an otherwise bare charge
- effect of cylindrical bare charge length to diameter (L/D) ratio
- effect of cylindrical pipe bomb L/D with sand fragment restraint

In these shots, the charges were supported at the center of the vessel sphere by stands fabricated from 1-in.-thick styrofoam of 2-lb/ft^3 density. The sand layers were supported by Styrofoam and thin cardboard or tape forms. For all non-spherical shots the charges were oriented with the charge axis of symmetry horizontal along the sphere centerline and parallel to the face of the door.

The spherical charges were initiated by detonators imbedded in the center of the charges. The cylindrical charges were initiated by detonators imbedded 1 to 1-1/2-in. in the end of the charges.

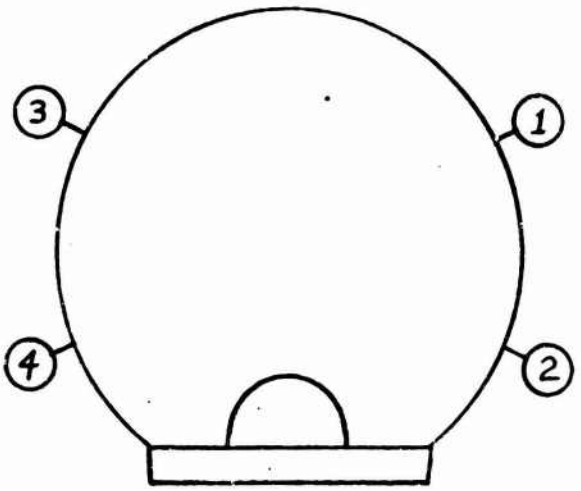

Top View

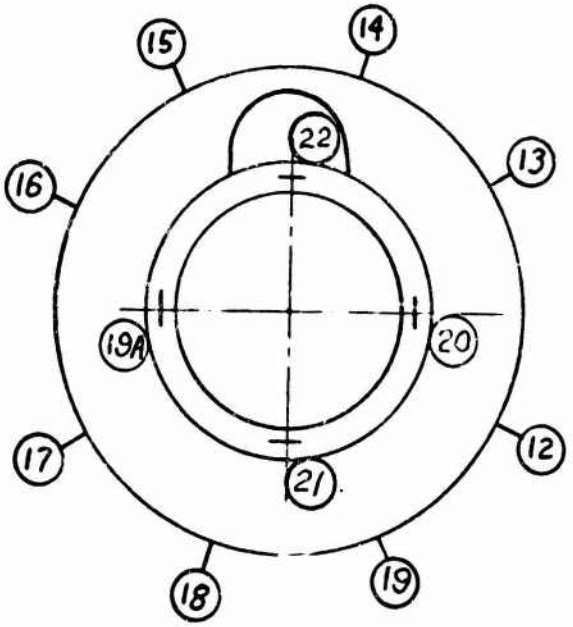

Front View

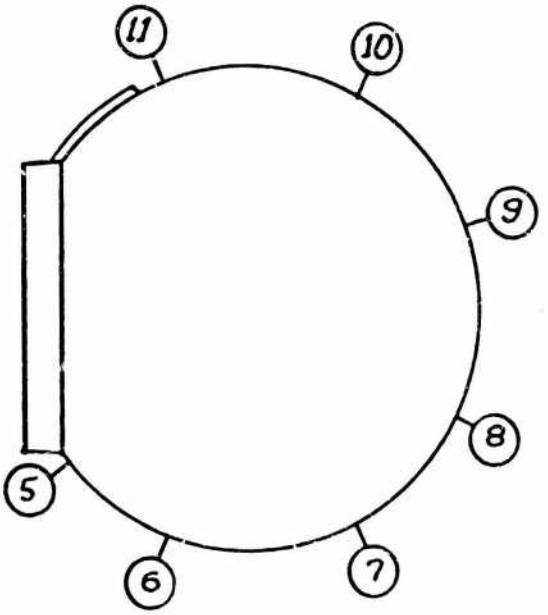

Right Side View

FIGURE 7. LOCATION OF FIDUCIAL MARKS ON THE VESSEL

TABLE 4. DESCRIPTION OF SHOTS FIRED

Shot Number	Explosive	Explosive Weight	Shape	Housing	Fragment Protection	Energy Absorber
1	C-4	1.59 lb	Sphere 3.71 in. dia.	none	none	none
2	C-4	2.56	Sphere 4.40 in. dia.	none	none	none
3.	C-4	1.52	Sphere 3.71 in. dia.	none	sand[a]	none
4	C-4	2.51	Sphere 4.40 in. dia.	none	none	#2 steel wool 16.9 lb
5	C-4	2.50	Cylinder L/D = 0.89	none	none	none
6	60% Dynamite	1.35[b]	Cylinder L/D = 3.88	8" x 2" pipe[c]	sand[a]	none
7	C-4	1.50	Cylinder L/D = 3.84	none	none	none
8	C-4	1.50	Cylinder L/D = 7.82	none	none	none
9	C-4	1.50	Cylinder L/D = 3.88	8" x 2" pipe[c]	sand[a]	none
10	C-4	1.50	Cylinder L/D = 8.14	13.1" x 1 1/2" pipe[d]	sand[a]	none

Notes: (a) Sand radial thickness 2.5 in. in contact with charge or housing.
(b) Two sticks
(c) Schedule 40 pipe with standard pipe caps on the ends
(d) Schedule 40 pipe with end plugs fitted inside cut from standard pipe caps.

The measured results of the tests include:

- the dynamic response of the vessel as measured on 4 strain gages.
- the static strain at each gage station as measured by the six strain gages
- the plastic deformation of the vessel as measured by the set of fiducial marks.

In addition to these measurements, the vessel was visually examined for fractures or failures after each shot and photographed from several angles after Shots 6 and 10.

Table 5 shows the first cycle peak dynamic strains as measured from the oscilloscope photographs. Initially, gage Nos. 1-4 were monitored. After Shot No. 4, the heated steel wool settled into the bottom of the vessel which raised its temperature beyond the tolerance of gage No. 3 located nearest to the bottom of the vessel causing the gage to peel away from the vessel. The nominal temperature tolerance of this gage and cement should be at least 400 F. Gages 1, 2, 4, and 6 were monitored dynamically on Shots 5-9 inclusive. After Shot 9, gage No. 2 was found to have 1/3 of its active area unbonded from the vessel surface, presumably because of exceeding the maximum strain limit of the EPY-500 cement used. In Shot 10, gages 1, 4, 5 and 6 were monitored dynamically.

Table 6 shows the strain gage readings obtained statically after each shot. The loss of gage No. 3 after Shot 4 and gage No. 2 after Shot 9 was described previously.

Table 7 shows the measured length changes of the fiducial gage lengths for each shot together with cumulative values for the test series.

It may be remarked that the large strain observed by gage No. 2 after Shot 5 is apparently quite real although the fiducial gage lengths near this gage do not show the large strain recorded by the gage. Shot 5 was fired with the detonator cap in the charge located at the end opposite to the end closest to gage No. 2. In this shot there was an obvious detonation direction effect leading to the production of a localized visible bulge almost centered on the gage, but not extending appreciably into the lines between nearby fiducial marks.

TABLE 5. PEAK DYNAMIC FIRST CYCLE STRAINS, MICROSTRAIN

Shot No.	Gage No. 1	Gage No. 2	Gage No. 3	Gage No. 4	Gage No. 5	Gage No. 6
1	1910	1511	2230	1486		
2	2031	2883	off scale >4300	2085		
3	2871	8675	7280	1378		
4	4307	8343	4981?	1440		
5	3137	off scale >9250	--	1821		4433?
6	4308	5063	--	1394		2664
7	4534	1481[b]	--	2774		1399[a]
8	4383	2947	--	2354		1162[c]
9	5275	12620	--	3531		5034
10	6620	--	--	4600	2932	2788[d]

(a) Larger 2nd cycle strain of 3485
(b) Larger 2nd cycle strain of 1950
(c) Larger 2nd cycle strain of 3330
(d) Larger 2nd cycle strain of 3098
? Possibly off scale. This is highest measurable value.

TABLE 6. STATIC STRAIN GAGE READINGS, MICROSTRAIN

Shot No.	Gage No. 1	Gage No. 2	Gage No. 3	Gage No. 4	Gage No. 5	Gage No. 6
Before	0	0	0	0	0	0
1	-520	-81	1144	201	-174	-305
2	-1034	656	12422	850	100	-827
3	-1926	8877	17684	984	2340	9271
4	589	14109	open	852	5444	13020
5	1022	39978	--	863	6387	15630
6	2640	41740	--	662	7421	14754
7	4270	40661	--	1118	8352	15939
8	6358	40304	--	1501	10363	16134
9	8112	43964	--	1008	11317	16684
10	10841	--	--	1446	13024	15396

Note: All readings taken with vessel at 70 ± 30° F.

TABLE 7. RESULTS OF FIDUCIAL MARK READINGS

Mark Pair	Original Length Inches	Length Changes on Each Shot, Mils										Total Change	
		No. 1	No. 2	No. 3	No. 4	No. 5	No. 6	No. 7	No. 8	No. 9	No. 10	Mils	Percent
1-2	9.489	?	16	42	21	8	-1	6	-1	16	14	124	1.31
3-4	8.228	2	14	42	20	12	-4	10	-10	0	9	95	1.15
5-6	6.045	8	2	30	18	18	84	21	8	195	99	479	7.92
6-7	9.389	-6	43	39	9	51	140	49	9	176	48	558	5.94
7-8	9.441	35	99	117	12	79	191	55	32	235	170	1025	10.85
8-9	8.982	0	64	89	36	59	150	30	15	226	65	734	8.17
9-10	9.174	-6	45	101	54	52	170	18	8	270	58	770	8.39
10-11	9.607	0	23	53	56	35	196	22	14	131	144	674	7.02
12-13	8.910	-5	17	27	0	20	-9	4	-3	22	27	110	1.23
13-14	9.096	1	6	36	12	21	-21	10	1	-19	20	67	.74
14-15	9.193	1	16	26	7	-2	-72	0	13	-1	39	27	.29
15-16	9.058	-3	20	69	14	14	2	10	9	22	-17	143	1.58
16-17	9.295	1	15	59	16	30	-23	8	-4	1	14	117	1.26
18-19	8.559		7	89	0	-2	-38	-8	8	-23	10	72	.84
19A-20	-12.84	4	22	5	4	11	-15	-18	-36	-67	1	-92	-.71
21-22	-13.28	3	0	0	0	6	15	38	31	114	31	248	1.86

Table 8 shows the plastic strain distribution data obtained from the fiducial mark readings shown in Table 7. Also shown in Table 8 are the overall average strains from the vessel skin fiducial marks and two other partial averages to help assess the effect of the charge shape on the vessel response. The End Average is the average of the strains between fiducial mark pairs 1-2, 3-4, 12-13, and 16-17. Reference to Figure 7 shows that these gage lengths extend across the portions of the vessel opposite the ends of the cylindrical charge shapes. The Side Average is the average of strains between fiducial mark pairs 5-6, 7-8, 8-9, 9-10, 10-11. These gage lengths lie in a great circle opposite the sides of the cylindrical charges. The Side/End Ratio shown in Table 8 is simply the ratio of the Side Average to End Average strains.

It will be noted that if the vessel response to spherical charges were spherically symmetric the Side/End Ratio should equal unity. The response of the vessel does not show such spherical symmetry as the Side/End Ratio reveals for spherical Shots 1-4. However the Side/End Ratio departs much further from unity for the cylindrical charges as an indication of the charge shape effect. In some cases the ratio is negative because the End Average strain is negative. This effect will be discussed later.

Figures 8, 9, and 10 show similar views of the vessel taken after Shot 6, the first pipe bomb shot, and after Shot 10. Of particular note in Figure 8 are the two localized bulges on either side of the weld along the top profile of the photo. More generalized strain in these areas largely obliterated the appearance of these bulges in later shots. They were probably caused by the impact of large fragments from the pipe bomb. No surface disturbance by the fragment impact was caused on the inside however. In Figure 8b, the general swelling of the vessel along the vertical plane between the caster wheels is apparent. One caster wheel was lost during Shot 10. The nut securing the wheel in place was found to have stripped threads as the source of failure. Previously, on Shot 7, a segment of about 120 degrees was broken out of the tire on the same caster. The fracture occurred through the rubber portion only.

Comparison of the vessel appearance in Figures 9a and 9b, and 10a and 10b reveals the nonuniform nature of the strain produced by the cylindrical charges.

TABLE 8. PLASTIC STRAIN DISTRIBUTIONS

Fiducial Mark Pair	Original Length, In.	Strain on Each Shot, percent										Total Change	
		No. 1	No. 2	No. 3	No. 4	No. 5	No. 6	No. 7	No. 8	No. 9	No. 10	Mils	Percent
1-2	9.489	.03	.17	.44	.22	.08	-.01	.06	-.01	.17	.15	124	1.31
3-4	8.228	.02	.17	.51	.24	.15	-.05	.12	-.12	.00	.11	95	1.15
5-6	6.045	.13	.03	.50	.30	.30	1.39	.35	.13	3.22	1.57	479	7.92
6-7	9.389	-.06	.46	.41	.10	.54	1.49	.52	.10	1.88	.51	558	5.94
7-8	9.441	.37	1.05	1.24	.13	.84	2.02	.58	.34	2.49	1.80	1025	10.85
8-9	8.982	.00	.71	.99	.40	.66	1.67	.33	.17	2.52	.72	734	8.17
9-10	9.174	-.06	.49	1.10	.59	.57	1.85	.20	.09	2.94	.63	770	8.39
10-11	9.607	.00	.24	.55	.58	.36	2.04	.23	.15	1.36	1.50	674	7.02
12-13	8.910	-.06	.19	.30	.00	.22	-.10	.04	-.03	.25	.30	110	1.25
13-14	9.096	.01	.07	.40	.13	.23	-.23	.11	.01	-.21	.22	67	.74
14-15	9.913	.01	.17	.28	.08	-.03	-.78	.00	.14	-.01	.42	27	.29
15-16	9.058	-.03	.22	.76	.16	.16	.02	.11	.10	.24	.19	143	1.58
16-17	9.295	.01	.16	.64	.17	.32	-.25	.09	-.04	.01	.15	117	1.26
18-19	8.559	NR	.08	1.04	.00	-.02	-.44	-.09	-.09	-.27	.46	72	.84
19A-20	12.84	.03	.17	.04	.03	.09	-.12	-.14	-.28	-.52	1.01	-92	-.71
21-22	13.28	.02	.00	.00	.00	.04	.11	.29	.23	.86	.23	248	1.86
Overall Skin Average		.029	.301	0.655	.221	.312	.616	.189	.065	1.042	.624		4.05
End Average			.172	.472	.159	.194	-.102	.079	-.052	.107	.178		
Side Average			.497	.799	.349	.544	1.744	.368	.161	2.401	1.123		
Side/End Ratio			2.87	1.690	2.19	2.802	-17.10	4.66	-3.08	22.49	6.23		

a. After Shot #6

b. After Shot #10

FIGURE 8. SIDE VIEWS OF VESSEL

a. After Shot #6

b. After Shot #10

FIGURE 9. REAR VIEWS OF VESSEL

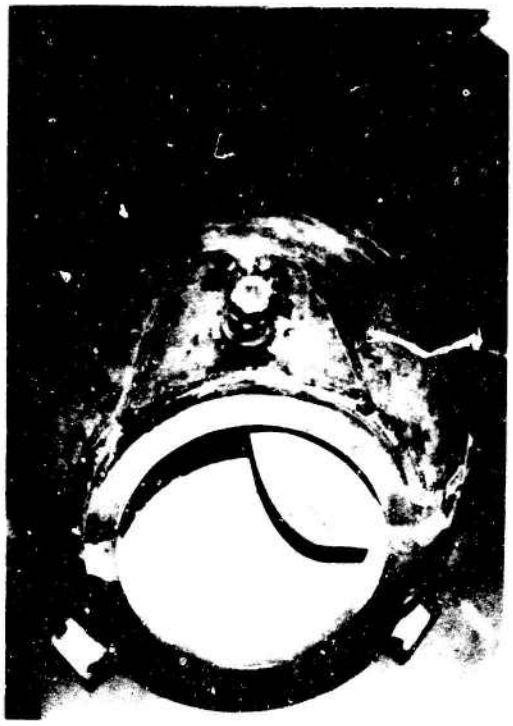

a. After Shot #6

b. After Shot #10

FIGURE 10. FRONT VIEWS OF VESSEL

Figure 10 shows the location of the crack produced by Shot 10, located just below the port. Also shown in Figure 10 is the smooth nature of the interior of the vessel. As expected, the 2.5-inch sand layer provided complete protection against the formation of fragment craters in the vessel surface.

Figure 11 shows two views of the crack in the vessel produced by Shot 10. The crack did not open appreciably, as evidenced by the nearly 30 seconds venting time for the contained gases observed for Shot 10. The crack comes within about 1/16-inch of the weld metal on both the outside as shown and also on the inside of the vessel. The maximum displacement of the crack edges with respect to each other is approximately 3/16-inch.

DISCUSSION

An elastic-plastic computer program (1,2) to predict the performance of spherical blast-containment vessels has been developed at Battelle as an aid to understanding the performance of spherical blast containment chambers. The program uses a bilinear elastic-plastic model with linear work hardening for the stress-strain behavior of the metal. Due to uncertainties in the effect of strain rate on the material properties, especially the yield strength, these parameters are currently treated as adjustable parameters to make the predicted results agree with experiments. This code has demonstrated good agreement with the average residual strains produced by large spherical C-4 charges in a series of vessels nominally identical to the one evaluated in this program.[1] To obtain agreement with experiment a yield strength of 80,000 psi was assumed. This value also appears to predict results in good agreement with the average strain of the vessel skin for the bare spherical C-4 shots in this program as shown in Figure 12. The error bars shown on the data points show the maximum and minimum strains recorded

a. Side View

b. Front View

FIGURE 11. VIEWS OF CRACK IN VESSEL AFTER SHOT #10

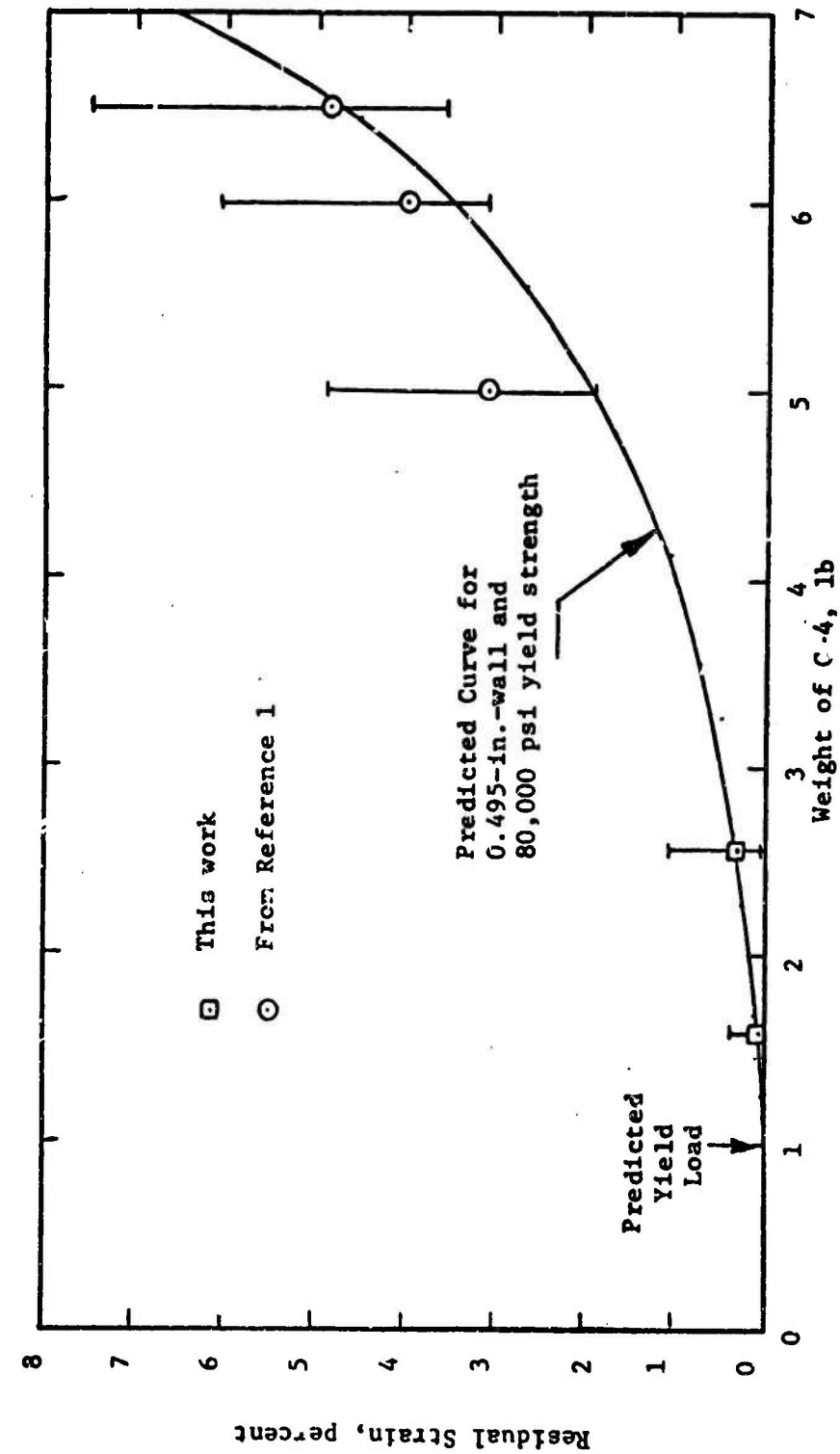

FIGURE 12. COMPARISON OF PREDICTED AND OBSERVED RESIDUAL STRAINS FROM SPHERICAL CHARGES

by individual fiducial gage lengths on each vessel. Although a strain-hardening effect is known[1] to exist for repeated shots, it is expected that the residual strain for the 1.56-lb Shot No. 1 was sufficiently small that no appreciable strain-hardening occurred as a result of this shot. However the 2.56-lb Shot No. 2 produced sufficient strain that strain-hardening effects are expected to be present in subsequent shots which would tend to reduce the observed strains below those which would have occurred if a new vessel had been employed for each shot. At present there is insufficient data to assess the magnitude of the strain hardening effect with certainty.

Shot No. 5 provides some indication that the strain-hardening effect in the vessel was still quite small, at this point in the test series. The average strain produced by Shot No. 5, a compact cylindrical charge with L/D = 0.89 was very close to that produced by Shot No. 2, a spherical charge of of the same weight. In addition, the Side/End Ratios given in Table 8, show that that this compact cylindrical shape is quite similar to a sphere in its effect on the vessel. One departure from this similarity was the small bulge produced near strain gage No. 2 described previously.

The 2.5-in. layer of sand around Shot No. 3 produced strains well in excess of that expected for a bare charge. If strain-hardening effects are ignored, the average strain produced was equivalent to a bare charge of $\sim$ 3.4 lbs. Inclusion of strain hardening has the effect of increasing the equivalent bare charge weight. It is not known at present how this effect of enhanced momentum transfer to the vessel wall by a surrounding sand barrier will scale with total charge load and relative sand barrier thickness.

If the premise that little strain hardening had occurred in the vessel when Shot No. 4, the steel wool energy absorber test shot, was fired, then it appears that the steel wool had a beneficial effect in reducing the strain produced by the 2.5-lb spherical C-4 charge. The average strain in the vessel produced by Shot No. 4 was $\sim$26.6 percent less than that produced in Shot No. 1. The specific explosive load in this experiment was $\sim$0.6 lb C-4 per ft^3 of containment volume. This is appreciably in excess of the specific loads of 0.08-0.15 lb C-4/ft^3 used by Gross, et al of Artec Assoc.[3]

Quantitative comparison of the present results with those of Gross, et al is difficult due to the different response regimes of their vessel (primarily elastic) and the present vessel (appreciable plastic deformation). However, qualitatively, it appears that the beneficial effects of the steel wool energy absorber, as used in these experiments is somewhat less than might have been expected based on their results. This is probably due to the higher specific explosive load and hence higher specific energy load tending to saturate the energy absorber rendering it relatively less effective.

The experimental method used in following the distortion of the vessel, i.e. chord measurements does not measure surface strains correctly when shape changes in the vessel occur. However, measurements taken along the vessel surface which could measure the strain in the outer layer of the vessel skin would not reveal information regarding shape changes in the vessel either. At least a three-point measurement along the vessel surface would be required plus a significant analytical effort to evaluate energy absorption due to bending. These measurements and the associated analysis were beyond the scope of the present program.

Nevertheless significant data regarding the effect of charge shape has been obtained. It is quite clear that cylindrical charges produce a highly anisotropic shock wave field and that the vessel responds to this large anisotropy. Although qualitative, the Side/End Ratio figures given in Table 8 are at present the best measure available for this anisotropy which is superposed on the non-uniform response of the vessel to spherical charges. It is obvious that as the End Strain Average gets smaller, the Side/End Ratio will increase, and that for a zero End Strain Average the Side/End Ratio is infinity. Further decreases in the End Average to negative values leads to negative Side/End Ratios which should be interpreted as larger measures of distortion anisotropy.

A short analysis presented in Appendix A shows that under certain conditions straightening of a spherical cap of finite thickness can lead to reductions in a measured chord length on the outside of the cap corresponding to the chord length measurements used in this program. Thus, negative chord

length changes are the result of straightening effects predominating over internal blast loading stretching effects.

Precise comparisons of the anisotropic effects of the various charges fired in this program were precluded by the cumulative change in the vessel shape with the repeated firing of cylindrical charges. The results do appear to be in general agreement with the hypothesis that greater L/D ratios lead to larger anisotropic effects, and that the presence of a steel and sand barrier on the outside of the cylindrical charges further enhances the anisotropic effect over that of bare charges.

REFERENCES

(1) Trott, B. D., Backofen, J. E., and White, J. J., "Design of Explosion Blast Containment Vessels for Explosive Ordnance Disposal Units", Final Report (June, 1975), from Battelle Memorial Institute to Picatinny Arsenal, Contract No. DAAA21-72-C-0129.

(2) Trott, B. D. and White, J. J., "An Elastic-Plastic Analysis of Spherical Blast Containment Chambers" (to be published).

(3) Gross, M. B., Gill, S. P., and Mihalik, G. R., "Feasibility of Explosive Blast Muffler Concepts", Final Report III, Artec Associates Inc., Hayward, Cal. 94545 (July 1974).

APPENDIX A

APPROXIMATE ANALYSIS OF STRAIGHTENING A SPHERICAL CAP

APPENDIX A

APPROXIMATE ANALYSIS OF STRAIGHTENING A SPHERICAL CAP

In this approximate analysis we consider a spherical cap of initial outer radius r_o which is straightened somewhat to spherical cap of larger radius r while maintaining the same gage thickness h, and volume V. The objective of this analysis is to determine the conditions under which an initial chord measurement C_o across the cap will become shorter upon partial straightening of the cap.

The initial volume of the cap is

$$V = \frac{2\pi}{3} (1 - \text{Cos}\theta_o) (r_o^3 - (r_o - h)^3), \tag{1-A}$$

where θ_o is one-half the original angle subtended by the cap.
The final volume of the cap is

$$V = \frac{2\pi}{3} (1 - \text{Cos}\ \theta) (r^3 - (r - h)^3). \tag{2-A}$$

Since the volume is unchanged on straightening, equations (1-A) and (2-A) were equated and solved for the new angle subtended θ for the new larger radius r:

$$\theta = \text{Cos}^{-1}[1 - (1 - \text{Cos}\theta_o) (1 - (1-y)^3/(x^3 - (x-y)^3)], \tag{3-A}$$

where

$$x = r/r_o$$
$$y = h/r_o$$

The original chord measurement C_o is given by

$$C_o = 2r_o \text{ Sin } \theta_o . \tag{4-A}$$

The new chord measuremend C is given by

$$C = 2r \text{ Sin } \theta . \tag{5-A}$$

From Equations (4-A) and (5-A) the fractional change is in the chord length is given by

$$\Delta C/C_o = (C - C_o)/C_o = r\text{Sin}\theta/r_o\text{Sin}\theta_o - 1 . \tag{6-A}$$

By insertion of the value of θ given by Equation (3-A) into Equation (6-A) it is seen that the fractional change in chord length is reduced to a function of the original half-angle subtended θ_o and the ratios $x = r/r_o$ and $y = h/r_o$:

$$\Delta C/C_o = x \, \mathrm{Sin}\left\{\mathrm{Cos}^{-1}\left[1 - (1 - \mathrm{Cos}\theta_o)\,(1 - (1-y)^3)/(x^3 - (x-y)^3)\right]\right\}/\mathrm{Sin}\theta_o - 1 \,. \qquad (7\text{-A})$$

A partial analysis of the properties of this rather complex equation was conducted for values of interest to this program. It was found that for all values of θ_o below some critical value, which depends on the values of both $y = h/r_o$, and $x = r/r_o$ that $\Delta C/C_o$ is negative.

The values of y of interest here span the range of wall thicknesses h which were measured, i.e. $0.444 \leqslant h \leqslant 0.569$. If we take $r_o = 12.0 + h$, the range of values of $y = h/r_o$ becomes $0.03568 \leqslant y \leqslant 0.04527$. Analysis of the properties of Equation (7-A) showed that the critical values of θ_o are larger for the larger values of y. The variation in θ_o (crit.) for which $\Delta C/C_o$ is negative for smaller values of θ_o with x is shown in the table below together with the accompanying values of the original chord length from Equation (4-A).

x	θ_o (crit)	max. C_o
1.01	17.09^o	7.39
2	19.86^o	8.54
3	21.10^o	9.04
10	23.26^o	9.93
50	24.14	10.28

Thus it is seen through this simplified analysis that for sufficient straightening of the spherical wall the finite thickness of the vessel can produce a negative change in an outside chord measurement, if the initial chord measurement and angle subtended is not too large. Comparison of the maximum chord lengths for a fractional reduction on straightening with the initial chord lengths used in this study as given in Table 7 shows them to be similar in length, but generally longer for the smaller amounts of straightening estimated to correspond to the straightening observed across the ends

of the vessel. Hence, although it is believed that this analysis has correctly identified the basic phenomena responsible for the observed chord length reductions, other effects must be operative in conjunction to fully understand the observed results. The other effects which are candidates are the known non-uniformity in wall thickness, the non-linear elastic-plastic properties of the vessel material, and residual stresses in the vessel walls following deformation.

APPENDIX B

WELDING PROCEDURE SPECIFICATION

WELDING PROCEDURE SPECIFICATION (WPS)

Welding Procedure Specification No./ Revisions P-75-A | Date 3/28/75 | Supporting PQR No(S) PQ-75-1

Welding Process(es) Gas-metal-arc in combination with shielded metal arc | Types Semi-automatic (GMA and Manual (SMA)

JOINTS

Groove design Single U

Backing

Other

BASE METALS

P No. 1 to P No. 1

Thickness range 3/16" to 3"

Other

FILLER METALS

F No. 4 and 6 Other

A No. 1 Other

Spec. No. SFA 5.20 (SFA, SFB) AWS No. E70T-1 (Class E7018)

Size of Electrode E7018 - 1/8" dia. E70T-1 - 3/32" dia.

Size of Filler

Flux Composition

Particle Size

Electrode Flux Composition

Consumable Insert

Other

POSITION

Position of Groove Flat

Welding progression

Other

PREHEAT

Preheat Temp. 250 F min.

Interpass Temp. 250 F min.

Preheat Maintenance

Other

POSTWELD HEAT TREATMENT

Temperature

Time Range

Other

WELDING PROCEDURE SPECIFICATION (WPS)
(Continued)

Welding Procedure Specification No. P-75-A Date 3/28/75

GAS

Shielding Gas(es) Carbon dioxide

Percent Composition _____ (mixtures)

Flow Rate 50 cfh

Gas Backing _____

Trailing Shielding Gas Composition _____

Other _____

ELECTRICAL CHARACTERISTICS

Current DC Polarity Reverse
AC or DC

Amps. E7018 160 to 180 E70T-1 380-400 (Range) Volts 26 volts E70T-1 (Range)

Travel Speed _____ (Range)

Other _____

TECHNIQUE PROCEDURES

String or Weave Bead String

Orifice or Gas Cup Size _____

Initial & Interpass Cleaning Initial: hand-held power grinder; Interpass: powered wire brush

Method of Back Gouging Power grinder

Oscillation _____

Contact Tube to Work Distance _____

Multipass or Single Pass Multipass (per side)

Single or Multiple Electrodes Single

Other _____

PROCEDURE QUALIFICATION RECORD (PQR)

Procedure Qualification Record No. PQ-75-1 Date 3/28/75

WPS No. P-75-A

Welding Process(es) Shielded metal-arc for passes 1 thru 4, gas metal-arc for balance Types Semi-Auto (GMA) and Manual (SMA) (Manual, Automatic, Semi-Auto.)

JOINTS

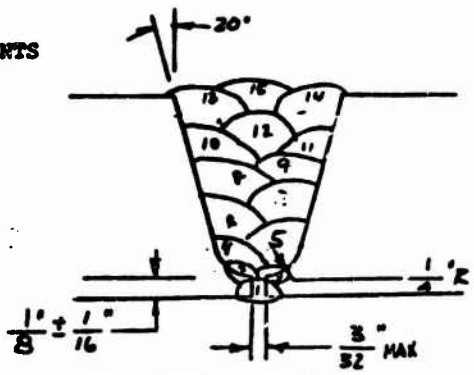

Groove Design Used

BASE METALS

Material Spec. A537A

Type or Grade

P No. 1 to P No. 1

Thickness 1-1/2 inches

Diameter

Other

FILLER METALS

Weld Metal Analysis A No. 1
Size of Electrode E7018 1/8"; E70T-1 3/32"
Filler Metal F No. 4 and 6
SFA Specification 5.5 and 5.20
AWS Classification E7018 and E70T-1
Other

POSITION

Position of Groove Flat
Weld Progression (Uphill, Downhill)
Other

PREHEAT

Preheat Temp. 250 F
Interpass Temp. 250 F
Other

POSTWELD HEAT TREATMENT

Temperature
Time
Other

GAS

Type of Gas or Gases Carbon dioxide
& Composition of Gas Mixture
Other 50 cfh

ELECTRICAL CHARACTERISTICS

Current DC
Polarity Reverse
Amps. * Volts 26 volts - E70T-1
Travel Speed
Other

TECHNIQUE PROCEDURES

String or Weave Bead String
Oscillation
Multipass or Single Pass Multiple (per side)
Single or Multiple Electrodes Single

* 170 amps 7018
380-400 amps E70T-1

PROCEDURE QUALIFICATION RECORD (PQR) PQ-75-1 3/28/75
(Continued)

TENSILE TEST RESULTS
SPECIMEN DIMENSIONS PER FIGURE QW 462.1d, Section IX, ASME Boiler Code

Specimen Number	Dimensions Width(1)	Dimensions Thickness(2)	Area sq. in.	Ultimate Load, lb	Stress, psi	Character and Location of Failure
1			0.202	16,025	79,406	Weld metal
2			0.202	15,925	78,880	Base metal
3			0.200	16,000	79,880	Base metal
4			0.201	15,750	78,511	Base metal

(1) Record outside diameter if a full pipe section is tested.
(2) Record wall thickness if a full pipe section is tested.

GUIDED BEND TEST RESULTS
SPECIMEN DIMENSIONS PER FIGURE QW 452.2a, Section IX, ASME Boiler Code

Specimen Number	Type	Bend Radius	Results	Specimen Number	Type	Bend Radius	Results
1	Side	1-1/4"	No defects	4	Side	1-1/4"	No defects
2	Side	1-1/4"	No defects				
3	Side	1-1/4"	No defects				

Toughness Tests

Specimen No.	Notch Location	Notch Test Type	Notch Test Temp.	Impact Values	Lateral Exp. %Shear	Lateral Exp. Mils	Drop Weight Break	Drop Weight No Break

Type of Test _____
Deposit Analysis _____
Other _____

Fillet Weld Test

Result - Satisfactory _____ (Yes, No) Penetration into Parent Metal _____ (Yes, No)

Type and Character of Failure _____ Macro Results _____

Remarks

The results of the bend and tensile tests met the requirements of Section IX, ASME Boiler and Pressure Vessel Code, 1974. Welds made by W.H. Stefanov.